ISSN 1330-3651 (Print), ISSN 1848-6339 (Online)
https://doi.org/10.17559/TV-20220403200857
Original scientific paper

Multi-Tooth Contact Analysis and Tooth Profile Modification Optimization for Cycloid Drives in Industrial Robots

Haidong HE, Xuan LI*, Ting ZHANG

Abstract: Cycloid drives are widely used in industrial robots where high load carrying capacity, accurate positioning precision and smooth motion are required strictly. The meshing clearance obtained by tooth profile modifications of cycloid gears is thought to have significant effects on performances of cycloid drives. In this study, this issue is clarified by developing a quasi-static load distribution model with considering four types of tooth profile modifications. Firstly, the unloaded tooth contact analysis is introduced to determine the meshing information, and the nonlinear Hertzian contact mechanics is applied to develop force-displacement relationships, Then, the loads distributed on gears, contact stress, loaded transmission error and gear ratio are calculated by enforcing the deformation compatibility, and force and moment equilibrium conditions. The predicted contact stress and deformation are compared with those by the finite element method, which shows a good agreement. With this, a tooth profile modification optimization method is proposed to obtain the optimal tooth profile modification at given radial clearances by using the two-dimensional parameter map. This study provides a useful tool to predict the multi-tooth contact conditions and to determine the most suitable tooth profile modification during the design process.

Keywords: contact stress; cycloid drive; multi-tooth contact; tooth profile modification; transmission error

1 INTRODUCTION

Nowadays, increasing industrial robots are used in a variety of tasks such as transporting, welding, grinding, and assembling through variable programmable motions. As shown in Fig. 1, the RV speed reducer is becoming more prominent for the use in industrial robots because of the advantages of large gear ratio, lightweight, high torsional rigidity [1]. Unlike more commonly understood involute gearing, it is a complicated eccentric rotation type planetary differential reduction mechanism. RV speed reducers consist of the involute gear drive and the cycloid drive, which determines directly the performance of the robot. Despite the increasing popularity, there are currently no available design standards and technical details for cycloid drives [2].

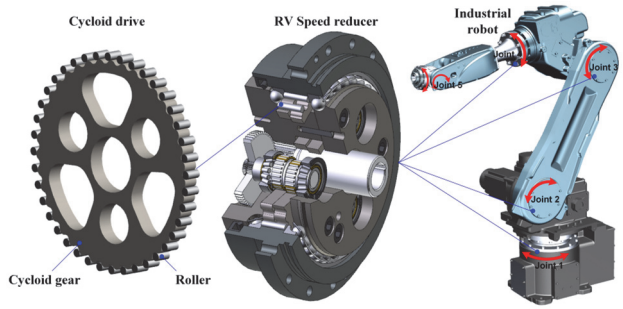

Figure 1 The structure of cycloid drives applied in the industrial robot

Cycloid drives have an ability to transfer large torques at small sizes with accurate positioning precision and smooth motion due to the multi-tooth contact characteristic. Theoretically, all gear teeth mesh with subsequent rollers placed at equal intervals on the ring gear and half of the rollers are considered to transfer the torque at any instance. In practice, the cycloid gear is usually manufactured to obtain an appropriate degree of clearance to adapt to the interferences due to manufacturing errors, contact deformations and thermal effect. The clearance can also be used for oil film forming and easier assembling [3]. Consequently, the cycloid gear with various types of tooth profile modifications impedes the theoretical tooth contact condition leading to the uncertain changes of the contact region, the number of meshing teeth pairs and the loads distributed among teeth pairs both in magnitude and direction. Tooth profile modifications (TPMs) of the cycloid gear have effects on the tooth contact strength, loaded transmission error and gear ratio fluctuation of cycloid drives.

Literature review shows that the valuable technical information on the TPM of cycloid gear is hardly available in the open literature pertaining to the modification determination and effects analysis, so many researchers are focused on the cycloid gear design [3-8], dynamic and kinematic characteristics analyses [9-14], efficiency and lubrication [15-17] of cycloid drives. Yang and Blanche [4] recommended that the roller radius should be modified to account for the cycloid gear tolerance. In contrast, Sensinger et al. [5] considered mathematically that the tooth profile curve can be obtained by changing the parameters of roller position and roller radius. Lin et al. [6] investigated the TPM of cycloid gears quantitatively under individual as well as combined conditions. Malhotra et al. [7] calculated the load distributed among predict the loads on various components of the speed reducer where under the assumption of perfect geometry and contact of rigid bodies. Gorla et al. [3] presented a method to analyse the load distributed on the components of a cycloid speed reducer and the theoretical results are validated by an experiment. Blagojevic et al. [8] developed an approximate approach for the multi-tooth contact analysis of a new two-stage cycloid speed reducer based on Malhotra's method. Li et al. [9, 10] proposed an analytical method to calculate the contact stress and stiffness, transmission error and gear ratio of a cycloid speed reducer with considering the effects of TPM and eccentric error. Xu et al. [11, 12] developed a contact dynamic model of cycloid drives to analyse the load distribution with considering the cylindrical roller bearing effects. Sun et al. [13] conducted a tooth contact analysis on a new type of CBR reducer based on the method of discrete point of tooth profiles. Lin et al. [14] proposed a method for the design and analysis of the transmission error the manufacturing tolerance. Li et al. [15] proposed a multi-tooth contact analysis model for cycloid drives applied in RV speed reducers with considering the manufacturing error effect. Hsieh et al. [16] presented a prediction method to estimate the stability and

power loss for various designs of cycloid speed reducers by using finite element method (FEM) implemented in the SolidWorks software. Wang et al. [1] proposed multi-tooth contact and transmission error models by dividing the contact area of tooth pairs into several differential elements. Li [17] developed a FEM program to analyse the tooth contact characteristics of the cycloid drive. Kumar et al. [2] proposed a method to determine the elastic torsional stiffness of cycloid drives on the experimental studies. Kim et al. [18] conducted the force and torsional rigidity analyses of cycloid drives based on the FEM and Hertzian contact theory.

When considering TPM effects on the performance of the cycloid drive, it is necessary to have an effective method to analyse the multi-tooth contact characteristics and to determine the optimum TPM to improve the performance. Therefore, a load distribution model is proposed to calculate the load distributed among rollers, contact stress, transmission error and gear ratio. With this, a two-dimensional parameter map is used to obtain the optimum tooth profile modification at given radial clearances. This study is aiming to provide a useful tool to predict the multi-tooth contact conditions, and to determine the most suitable tooth profile modification.

The rest of this paper is structured as follows: section 2 presents the geometrical design of the cycloid gear. In this section, the definitions of four individual and combined tooth profile modifications, the constraints of TPM amounts, and the radial as well as the normal clearances are studied thoroughly. Section 3 presents a load distribution model for cycloid drives with TPM. Section 4 offers a numerical example to verify the proposed model where calculation results for an example cycloid gear pair with and without tooth profile modifications are presented and compared. The predicted contact stress is verified by comparing with the finite element method (FEM) results. In Section 5, based on the proposed model, the effects of combined tooth profile modifications on the maximum contact stress, mean transmission error and peak-to-peak gear ratio are investigated by using the two-dimensional parameter maps. Finally, a conclusion is made in Section 6.

2 CYCLOID GEAR TOOTH PROFILE GEOMETRY

2.1 Tooth Profile Generation

The cycloid gear tooth profile is the envelope to the family of planar circular curves based on the enveloping method, which is studied by many researchers [19-22]. Three coordinate systems are defined for the tooth profile generation of cycloid gear, as shown in Fig. 2a.

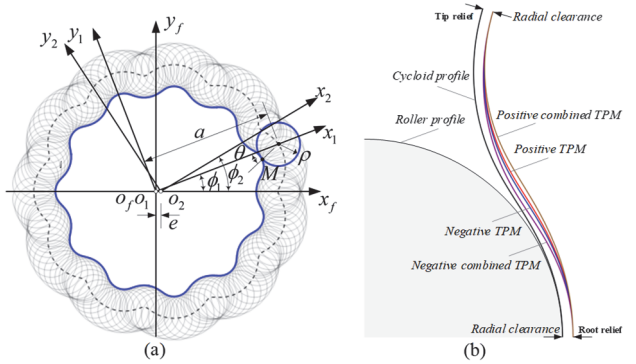

Figure 2 Cycloid gear (a) tooth profile generation and (b) modification

Two movable coordinate systems $S_1(x_1, y_1)$, $S_2(x_2, y_2)$, and a fixed coordinate system $S_f(x_f, y_f)$, stand for the pin-wheel, the gear and the gearbox, respectively.

The tooth profile equation of the cycloid gear can be represented in S_2:

$$\boldsymbol{r}_2(\theta,\phi_1)=\begin{bmatrix} a\cos(\phi_1/n_2)-\rho\cos(\theta-\phi_1/n_2) \\ -e\cos(n_1\phi_1/n_2) \\ a\sin(\phi_1/n_2)+\rho\sin(\theta-\phi_1/n_2) \\ -e\sin(n_1\phi_1/n_2) \\ 0 \\ 1 \end{bmatrix} \tag{1}$$

where, e is the eccentricity, a is the radius of roller position, ρ is the radius of rollers. Parameters ϕ_2 and ϕ_1 are the rotation angles having the relationship $\phi_2/\phi_1 = n_1/n_2$. the numbers of rollers and cycloid gear teeth are n_1 and n_2, where $n_1 + n_2 = 1$.

The equation of meshing is derived as:

$$f(\theta,\phi_1)=a\sin\theta-en_1\sin(\theta+\phi_1)=0 \tag{2}$$

2.2 Tooth Profile Modification

The mesh clearances of the cycloid gear can be designed in four ways by adjusting two parameters and in individual or combined conditions [1, 6]. Hence, the general equation of four modified profiles can be rewritten as:

$$\boldsymbol{r}_{2m}=\begin{bmatrix} (a+\Delta a)\cos(\phi_1/n_2)-(\rho+\Delta\rho)\cos(\theta_m-\phi_1/n_2) \\ -e\cos(n_1\phi_1/n_2) \\ (a+\Delta a)\sin(\phi_1/n_2)+(\rho+\Delta\rho)\sin(\theta_m-\phi_1/n_2) \\ -e\sin(n_1\phi_1/n_2) \\ 0 \\ 1 \end{bmatrix} \tag{3}$$

Fig. 2b illustrates the differences among the standard (unmodified) tooth profile and four modified tooth profiles. We can see that the four modified tooth profiles can achieve the same radial clearances c_r at the tip and root relief of one cycloid gear tooth, while the normal clearances c_n are quite different. The normal clearances c_n generated by modification amounts of Δa and $\Delta\rho$ for the four types can be derived as follows:

$$\begin{aligned} c_{n1} &= |\Delta a|\cos\theta_m, (\Delta a<0) \\ c_{n2} &= \Delta\rho, (\Delta\rho>0) \\ c_{n3} &= |\Delta a|\cos\theta_m - |\Delta\rho|, (\Delta a<0, \Delta\rho<0) \\ c_{n4} &= \Delta\rho - \Delta a\cos\theta_m, (\Delta a>0, \Delta\rho>0) \end{aligned} \tag{4}$$

where $\cos\theta_m = f(\phi_1) = \dfrac{1-\mu_m\cos\phi_1}{(1-2\mu_m\cos\phi_1+\mu_m^2)^{1/2}}$ is the function of ϕ_1.

To avoid the interference between the roller and cycloid gear tooth, the normal clearances c_{n3} and c_{n4} should be larger than zero. Therefore, the following constraints should be satisfied:

$$\begin{aligned} &|\Delta a|\, f(\phi_1)_{\min} - |\Delta\rho| > 0 \\ &\Delta\rho - \Delta a f(\phi_1)_{\max} > 0 \end{aligned} \tag{5}$$

Letting $f'(\phi_1) = \dfrac{\mu_m(\mu_m - \cos\phi_1)}{(1 - 2\mu_m\cos\phi_1 + \mu_m^2)} = 0,$ the minimum and maximum values of $f(\phi_1)$ can be derived as follows:

$$\begin{aligned} &f(\phi_1)_{\min} = (1-\mu_m^2)^{1/2}, \text{ when } \phi_1 = \arccos\mu_m \\ &f(\phi_1)_{\max} = 1, \text{ when } \phi_1 = 0 \end{aligned} \tag{6}$$

Therefore, the constraints for the four types can be given by,

$$\begin{aligned} &\Delta a < 0 \\ &\Delta\rho > 0 \\ &\Delta a < 0, \Delta\rho < 0, \Delta\rho - \Delta a(1-\mu_m^2)^{1/2} > 0 \\ &\Delta a > 0, \Delta\rho > 0, \Delta\rho - \Delta a > 0 \end{aligned} \tag{7}$$

3 LOAD DISTRIBUTION MODELLING

The load distribution modeling of cycloid drives based on the traditional rigid body or constant contact stiffness method typically assumes perfect geometries without clearances at all mesh phases [3, 7, 8]. This model lacks the ability to include tooth profile modification (TPM) effect accurately and fails to agree with the practical property of the gear mesh process.

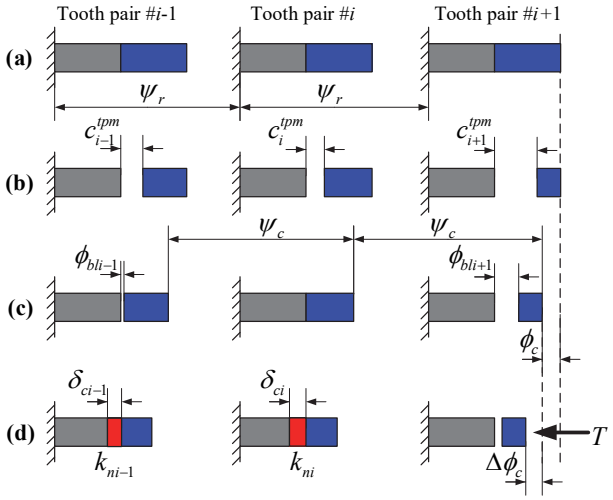

Figure 3 Schematic of contact conditions for multi-tooth pairs: (a) Theoretical contact; (b) Out of contact; (c) Rigid body contact; (d) Elastic body contact. (Keys: , contact positions on roller and gear respectively)

Fig. 3 shows the relative position relationships of multi-tooth pairs in different contact conditions during the mesh circle. In Fig. 3a, the theoretical contact condition of tooth pairs without TPM is shown. Fig. 3b shows that tooth pairs with different mesh clearances are in out-of-contact condition due to the TPM. The symbols ψ_r and ψ_c denote the constant angles between two adjacent rollers and cycloid gear tooth, respectively. The rollers are fixed while the cycloid gear can rotate freely. At least one tooth pair is always in contact as the cycloid gear with TPM rotates one certain angle ϕ_c, as shown in Fig. 3c. Also in Fig. 3d, once on the cycloid gear is applied with an external torque T, there will be a contact deformation δ_{ci} at the tooth pairs where the contact stiffness is k_{ni}. Then, further angular displacement $\Delta\phi_c$ of the cycloid gear occurs, and some of the backlash between gear pairs disappears and the number of meshing teeth pairs increases.

Based on the contact process mentioned above, the flowchart of the analysis on the load distribution for cycloid drives is shown in Fig. 4. Some assumptions for the model are the following:

1. The model is established in two-dimensional plane because the teeth are straight and parallel to the shaft axis.
2. The model is established under quasi-static condition with neglecting the inertia forces.
3. Friction can be neglected to avoid the uncertainness about Coulomb frictional coefficient.

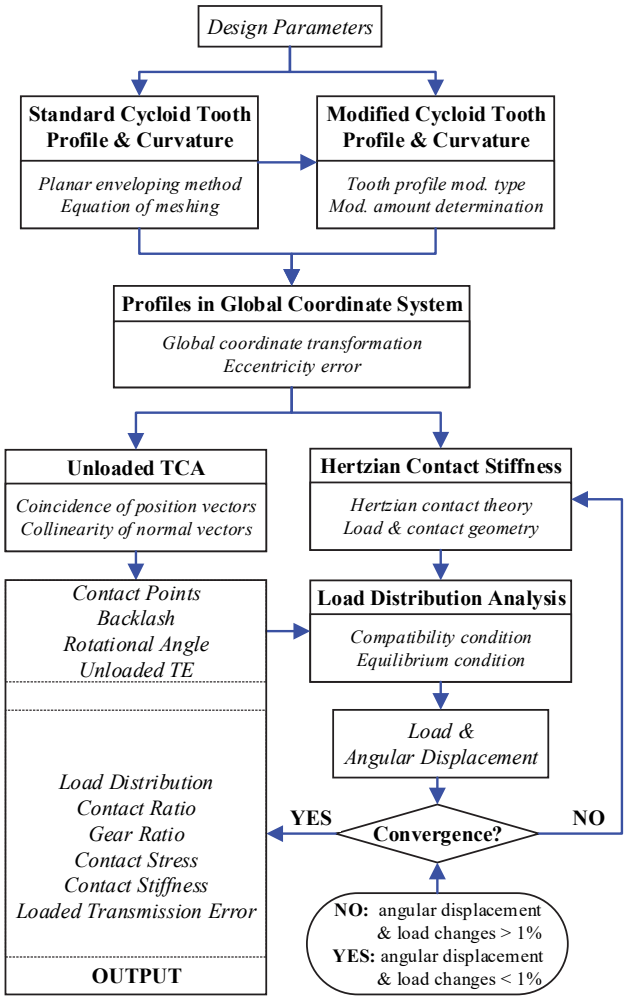

Figure 4 Flowchart of the load distribution analysis for the cycloid drive

3.1 Unloaded Tooth Contact Analysis Model

The unloaded tooth contact analysis (TCA) is a powerful tool to determine the meshing information, and it

has been successfully used for a cycloid pump [20]. As shown in Fig. 5, two coordinate systems $S_1(x_1, y_1)$ and $S_2(x_2, y_2)$ stand for the pin-wheel and cycloid gear, respectively. A fixed coordinate system $S_f(x_f, y_f)$ coinciding with S_1 is fixed.

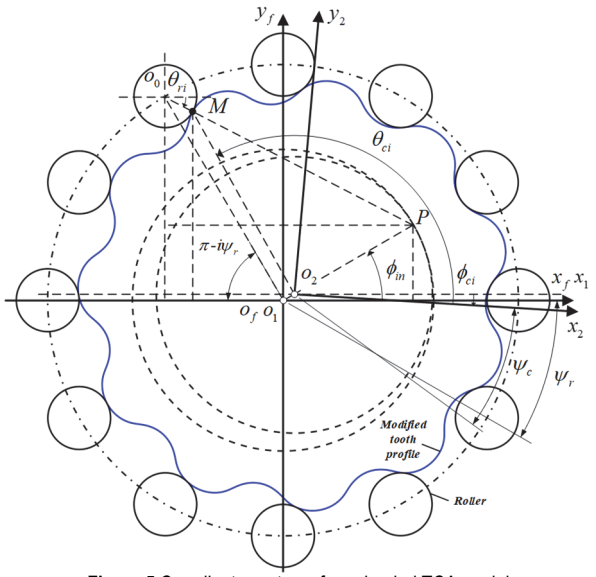

Figure 5 Coordinate systems for unloaded TCA model

Then, the position and normal vectors of roller profiles $\boldsymbol{r}_f^{(1)}(\theta_{ri})$ and $\boldsymbol{n}_f^{(1)}(\theta_{ri})$ can be expressed in S_f:

$$\boldsymbol{r}_f^{(1)}(\theta_{ri}) = \begin{bmatrix} \rho\cos(\theta_{ri}) + a\cos(i\psi_r) \\ -\rho\sin(\theta_{ri}) + a\sin(i\psi_r) \\ 0 \\ 1 \end{bmatrix} \tag{8}$$

$$\boldsymbol{n}_f^{(1)}(\theta_{ri}) = \frac{\dfrac{\partial \boldsymbol{r}_f^{(1)}(\theta_{ri})}{\partial \theta_{ri}} \times \boldsymbol{k}}{\left| \dfrac{\partial \boldsymbol{r}_f^{(1)}(\theta_{ri})}{\partial \theta_{ri}} \times \boldsymbol{k} \right|} \tag{9}$$

where i is the roller number, $\boldsymbol{k}$ = [0, 0, 1] is the unit vector and θ_{ri} is the angular parameter.

According to Eq. (3), the position vector $\boldsymbol{r}_f^{(2)}(\theta_{ci}, \phi_{ci}, \phi_{in})$ as well as its unit normal vector $\boldsymbol{n}_f^{(2)}(\theta_{ci}, \phi_{ci})$ can be expressed in S_f:

$$\begin{aligned} \boldsymbol{r}_f^{(2)}(\theta_{ci}, \phi_{ci}, \phi_{in}) &= \boldsymbol{M}_{f2}(\phi_{ci}, \phi_{in}) \boldsymbol{r}_{2m}^{(2)}(\theta_{ci}) \\ \boldsymbol{n}_f^{(2)}(\theta_{ci}, \phi_{ci}) &= \boldsymbol{L}_{f2}(\phi_{ci}) \boldsymbol{n}_2^{(2)}(\theta_{ci}) \end{aligned} \tag{10}$$

where ϕ_{ci} is the rotational angle of the cycloid gear, and

$$\boldsymbol{M}_{f2}(\phi_{ci}, \phi_{in}) = \begin{bmatrix} \cos\phi_{ci} & \sin\phi_{ci} & 0 & e\cos\phi_{in} \\ -\sin\phi_{ci} & \cos\phi_{ci} & 0 & e\sin\phi_{in} \\ 0 & 0 & 1 & 0 \\ 0 & 0 & 0 & 1 \end{bmatrix} \tag{11}$$

$$\boldsymbol{L}_{f2}(\phi_{ci}) = \begin{bmatrix} \cos\phi_{ci} & \sin\phi_{ci} & 0 \\ -\sin\phi_{ci} & \cos\phi_{ci} & 0 \\ 0 & 0 & 1 \end{bmatrix} \tag{12}$$

For performing the unloaded TCA, two contact conditions should be satisfied, which are the coincidence of position vectors and the collinearity of normal vectors of modified cycloid tooth and roller profiles at contact points. Therefore,

$$\begin{aligned} \boldsymbol{n}_f^{(1)}(\theta_{ri}) &= \boldsymbol{n}_f^{(2)}(\theta_{ci}, \phi_{ci}) \\ \boldsymbol{r}_f^{(1)}(\theta_{ri}) &= \boldsymbol{r}_f^{(2)}(\theta_{ci}, \phi_{ci}, \phi_{in}) \end{aligned} \tag{13}$$

Since the normal vectors $\left|\boldsymbol{n}_f^{(1)}\right| = \left|\boldsymbol{n}_f^{(2)}\right| = 1$, there are three independent nonlinear equations with four unknowns θ_{ri}, θ_{ci}, ϕ_{ci} and ϕ_{in} in the vector equations. When the input crankshaft angle ϕ_{in} is given, other unknowns will be solved by using Eq. (13).

Then, the backlash ϕ_{bli} and the rotational angle ϕ_c are represented as:

$$\phi_{bli} = \phi_c - \phi_{ci}, \ \phi_c = \max(\phi_{ci}) \tag{14}$$

In this paper, the backlash angle is defined as the amount of angular motion, which is necessary for all the mating tooth pairs to contact with each other so that torque can be shared among them.

3.2 Compatibility and Equilibrium Conditions

As shown in Fig. 6a, to determine contact points, the compatibility conditions can be expressed as:

$$\begin{aligned} &\text{in contact:} && \Delta\phi_c > \phi_{bli}, \alpha_i = \Delta\phi_c - \phi_{bli} \\ &\text{out of contact:} && \Delta\phi_c < \phi_{bli}, \alpha_i = 0 \end{aligned}$$

where $\Delta\phi_c$ is the rotational angle variation, and α_i is the angular displacement caused by the contact deformation.

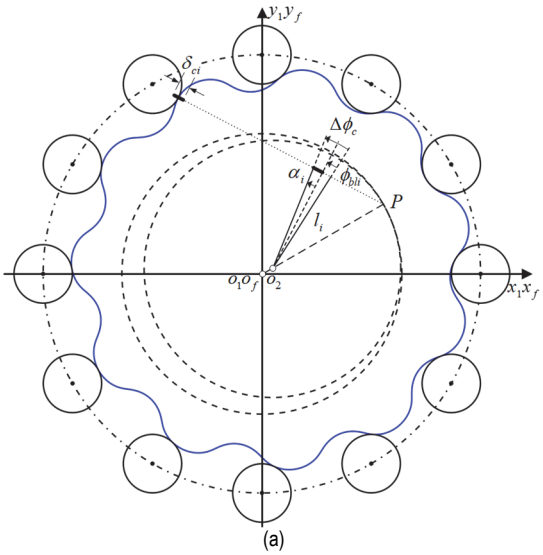

(a)

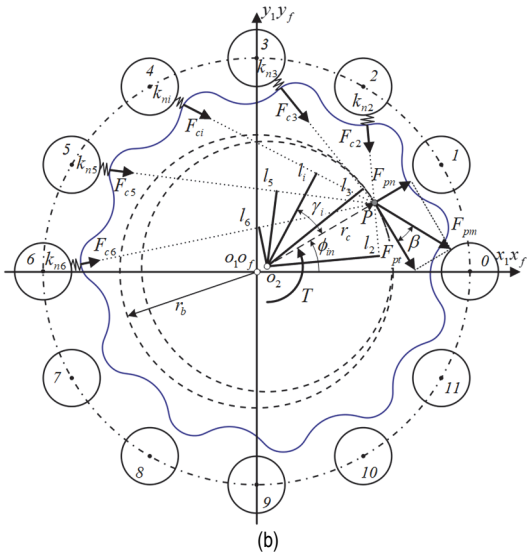

Figure 6 Compatibility and equilibrium conditions: (a) deformation compatibility; (b) force and moment equilibrium

As shown in Fig. 6b, the static equilibrium equations of the force and moment can be expressed as:

$$\begin{aligned} T &= \sum F_{ci} l_i \\ F_{ci} &= K_{ni} \delta_{ci} \\ \delta_{ci} &= \alpha_i l_i \\ & a\tan\theta_{ri}\cos i\psi_r - e\tan\theta_{ri}\cos\phi_{in} \\ l_i &= \frac{-e\sin\phi_{in} + a\sin i\psi_r}{\sqrt{\tan^2\theta_{ri}+1}} \end{aligned} \tag{15}$$

Then, the external torque can be rewritten as:

$$T = \sum K_{ni}\alpha_i l_i^2 \tag{16}$$

where K_{ni} is the mesh stiffness between the tooth and roller, which is used to establish the force-displacement relationships. In this paper, the nonlinear Hertzian contact stiffness is used instead of the constant contact stiffness, which can be represented as:

$$K_n = \frac{F}{\delta} = \frac{\pi B}{2\left[\frac{1-\nu_c^2}{E_c}\left(\ln\frac{4\rho_c}{b}-\frac{1}{2}\right)+\frac{1-\nu_r^2}{E_r}\left(\ln\frac{4\rho_r}{b}-\frac{1}{2}\right)\right]} \tag{17}$$

where b is the contact width and δ is the total deformation, which can be represented as:

$$\begin{aligned} b &= \sqrt{\frac{4F\rho^*}{\pi B E^*}} \\ \delta &= \frac{2F}{\pi B}\left[\frac{1-\nu_c^2}{E_c}\left(\ln\frac{4\rho_c}{b}-\frac{1}{2}\right)+\frac{1-\nu_r^2}{E_r}\left(\ln\frac{4\rho_r}{b}-\frac{1}{2}\right)\right] \end{aligned} \tag{18}$$

where B is the cycloid gear width, and

$$E^* = \frac{E_r E_c}{E_r(1-\nu_r^2)+E_c(1-\nu_c^2)} \text{ and } \rho^* = \frac{\rho_r\rho_c}{\rho_r+\rho_c}.$$

4 ANALYSIS RESULTS AND DISCUSSION

In this section, the proposed model is implemented by a computer program using MATLAB software, and analysis results for an example of cycloid drive with and without tooth profile modification (TPM) are presented and compared to show the effects of TPM. The basic design parameters and the TPM amounts are in Tab. 1.

Table 1 Design parameters and TPM amounts of the cycloid drive

Parameters	Descriptions	Values
n_2	Tooth number	39
n_1	Roller number	40
a	Roller position radius	64 mm
ρ	Roller radius	3 mm
e	Eccentricity	1.3 mm
B	Cycloid gear width	12 mm
Δa	TPM amount of a	5 μm
$\Delta\rho$	TPM amount of ρ	10 μm

There is an assumption that the material of cycloid gear and rollers is the same, which is the steel with the Poisson ratio ν = 0.3 and Young's modulus E = 206 GPa. The applied torque is set as 100 Nm.

4.1 Load Distribution and Contact Stress

The proposed quasi-static analysis can simulate the tooth contact of cycloid gear pair with time in the meshing circle. Thus, the load distribution among tooth pairs is calculated for contact stress estimation at 0°, 60°, 120° and 180° crankshaft angles. Fig. 7 and Fig. 8 show the comparison of calculated results between the cases with and without TPM. It is observed that a certain number of rollers mesh with the corresponding cycloid gear teeth, and the loads on the teeth change periodically within a mesh cycle. These multi-tooth contact characteristics explain the high load bearing capacity of cycloid drives. The maximum load is about 200 N on tooth No. 4 at crankshaft angle 0°, and almost half of tooth pairs participate in the torque transmission, for the case without TPM. However, for the case with TPM, large discrepancies are observed as the maximum load increases dramatically to 375 N on tooth No. 15 at crankshaft angle 120°, and the number of tooth pairs sharing the load decreases to 7 or 8.

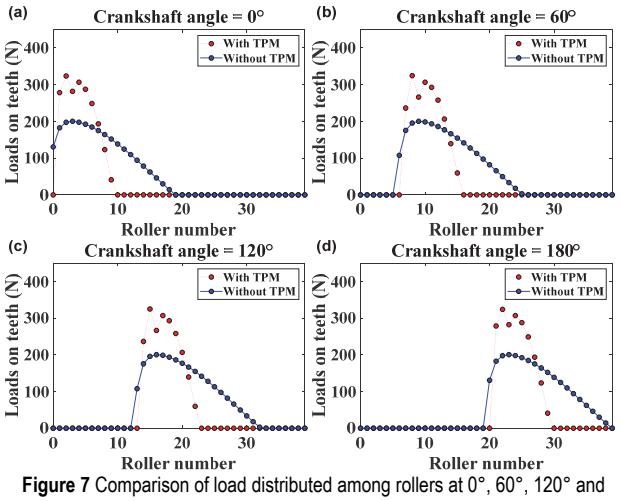

Figure 7 Comparison of load distributed among rollers at 0°, 60°, 120° and 180° crankshaft angles

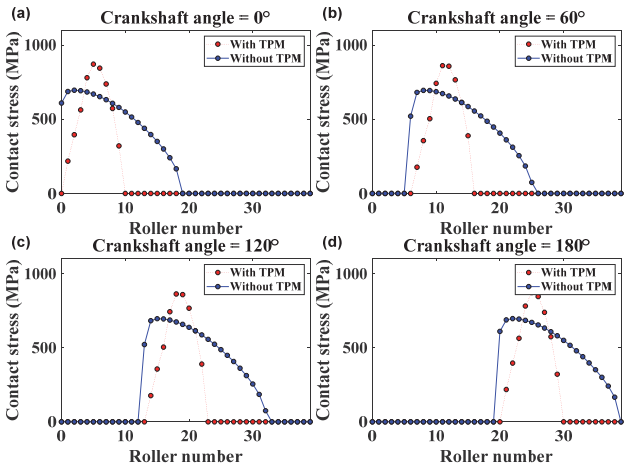

Figure 8 Comparison of contact stress on teeth at 0°, 60°, 120° and 180° crankshaft angles

One of the major concerns during the gear design process is the contact strength examination of the cycloid gear pair. The contact stress should be less than the limiting stress of the material. Based on the Hertzian contact theory, the stress σ is considered as the maximum contact pressure which can be represented as:

$$\sigma = \frac{2F}{\pi bB} \tag{19}$$

where contact width b is calculated according to Eq. (18).

Once the load and curvature radius at the contact point are calculated by the proposed model, the contact stress can be obtained according to Eq. (19). Fig. 8 shows the comparisons of the calculated results between the cases with and without TPM at 0°, 60°, 120° and 180° crankshaft angles. It is seen that the maximum contact stress does not occur on the same tooth pair where the maximum load is applied on due to the relative radius of curvature effect. For the case without TPM, the maximum contact stress is about 696.14 MPa. When the TPM is present, it increases to 901.73 MPa because of the number reduction of tooth pairs sharing the load.

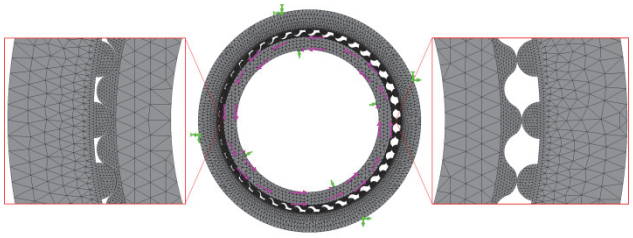

Figure 9 Finite element mesh, loading and boundary conditions of the cycloid drive

The comparative study of the proposed method with the finite element method (FEM) is done for the verification of the calculated results. The finite element analysis (FEA) software package, SolidWorks Simulation is applied for the static stress analysis. The three-dimensional model and material property of the cycloid gear pair with and without TPM have the same values of the parameters as the ones listed in Tab. 1. Fig. 9 shows the three-dimensional tetrahedral mesh with variable fineness and loading and boundary conditions. The area around the tooth pairs is refined for a high solution precision, as shown in the enlarged representations. The simulation analysis is conducted at the position where the crankshaft angle is 60° corresponding to the initial angular position.

Fig. 10 shows the comparison of contact stress on cycloid gear teeth and rollers without and with TPM. From the Von Mises stress contours, it is observed that there are twenty and seven tooth pairs sharing the load for the two cases, which agrees well with the obtained results from the proposed method shown in Fig. 8. The maximum contact stresses for cases without and with TPM are 795.64 MPa and 996.86 MPa, respectively, which shows a good agreement with the theoretically calculated results. The comparisons give an initial verification to the proposed load distribution model as the torque is applied.

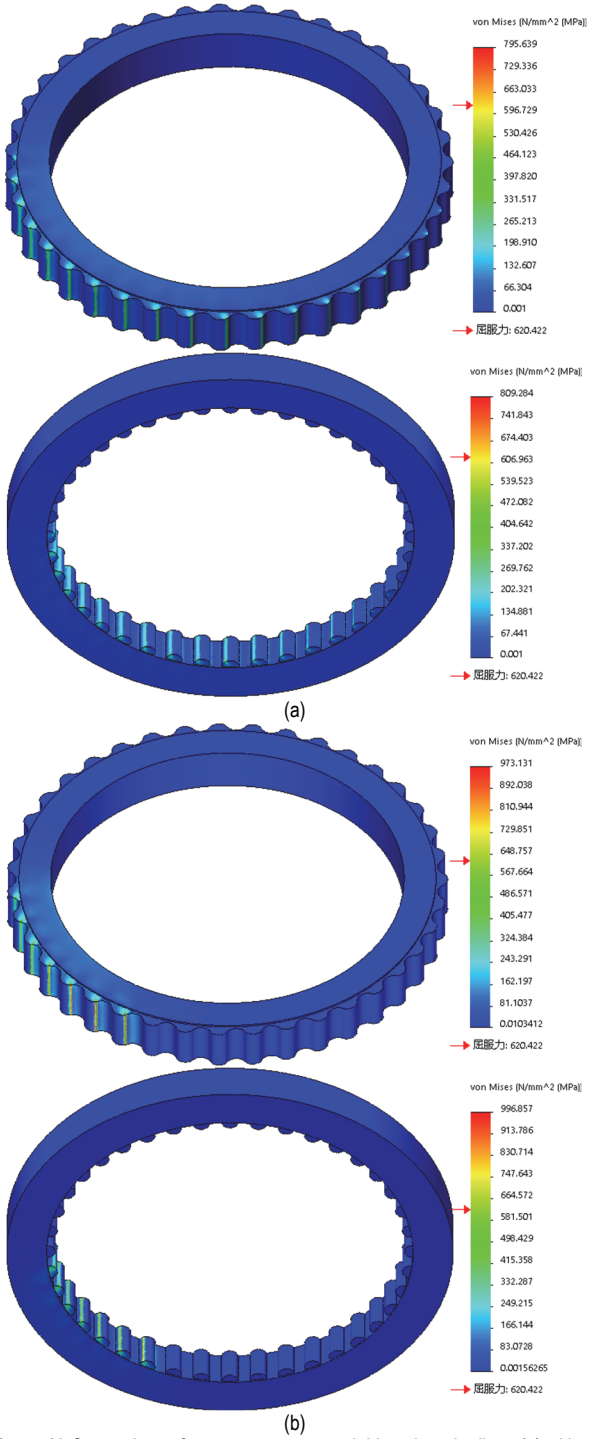

Figure 10 Comparison of contact stress on cycloid teeth and rollers: (a) without and (b) with TPM

4.2 Loaded Transmission Error and Gear Ratio

The loaded transmission error (*TE*) is the difference between the actual and theoretical rotational angle ϕ_a and ϕ_t of the cycloid gear, which is represented as:

$$TE = \phi_a - \phi_t \tag{20}$$

where $\phi_a = \phi_c - \Delta\phi_c$ and $\phi_t = -\phi_{in} / n_2$.

The actual gear ratio (*GR*) is defined as the ratio between output and input angular velocity while the ideal GR is a constant value, which equals the cycloid gear tooth number. Then, the actual *GR* can be represented as:

$$GR = \frac{\Delta\phi_a}{\Delta\phi_{in}} \tag{21}$$

where $\Delta\phi_a$ and $\Delta\phi_{in}$ are the increments of the actual output and input rotational angles.

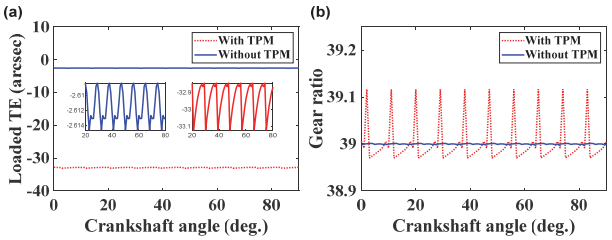

Figure 11 (a) the loaded transmission error and (b) actual gear ratio of cycloid drives

Fig. 11 shows the loaded *TE* and *GR* varying periodically as the input shaft rotates. The period of crankshaft angle equals the adjacent angle of two rollers, which is 9° in this case. It is observed that the TPM induces the increasing mean and peak-to-peak loaded *TE*, as shown in Fig. 11a. Also, the actual *GR* differs from the ideal *GR* (39), and the peak-to-peak *GR* is 0.3 due to the TPM and tooth deformation, as shown in Fig. 1b. This fluctuation of gear ratio will cause the torque ripple and resonance, which should be avoided in practical applications. The dynamic analysis is also desired to estimate the dynamic behaviour of reducers during the design process.

5 TOOTH PROFILE MODIFICATION OPTIMIZATION

Based on the discussion above, the TPM has significant effects on the maximum contact stress (MCS), mean transmission error (MTE) and peak-to-peak gear ratio (PPGR), which are associated with the load carrying capacity, the accurate positioning precision and the smooth motion of the industrial robot, respectively. Thus, it is necessary to determine the TPM in the design process of the cycloid drive. Different modification types and amounts should be applied for different applications due to different requirements of the lubrication and accuracy. However, no design criterion can be found in the open literature to determine the optimal TPM for cycloid drives.

In this section, based on the proposed load distribution model, a methodology for obtaining optimal TPM at given radial clearances is presented by using the two-dimensional parameters map for the minimization of the aforementioned design factors. Two types of combined modifications are considered. Based on the example gear pair, the maps of MCS, MTE and PPGR are generated with the absolute values of and ranging from 0 to 50 μm, as shown in Figs. 12, 13 and 14. The minimum values of design factors can be found in the dark blue zone where there is no TPM and the modification amounts are zero. However, in practice, the modification amounts are determined by the given radial clearance that depends on the oil film thickness and manufacturing errors. According to the maps, for each radial clearance c_r represented by the slant line, there is a minimum value of the MCS, MTE and PPGR corresponding to the combination of Δa and $\Delta\rho$, respectively.

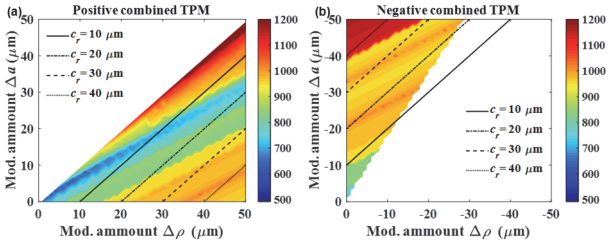

Figure 12 MCS for (a) positive and (b) negative combined TPM (unit: MPa, *T* = 50 Nm)

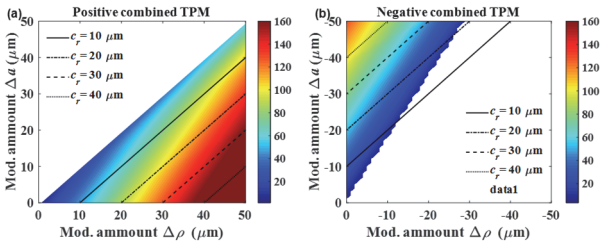

Figure 13 MTE for (a) positive and (b) negative combined TPM (unit: arc second, *T* = 50 Nm)

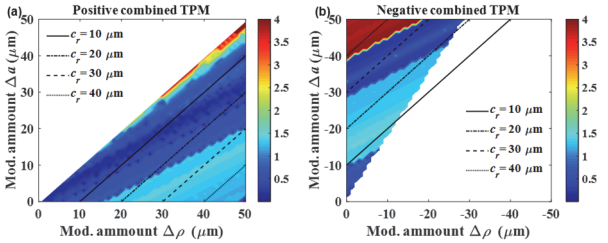

Figure 14 PPGR for (a) positive and (b) negative combined TPM (*T* = 50 Nm)

Taking the radial clearances at 10, 20, 30 and 40 μm as an example, the optimum modification amounts are determined by searching the minimum values of design factors on the slant lines of radial clearances in the maps and the optimization results are as listed in Tab. 2. From Tab. 2, the modification needed to minimize one of the above factors is often in conflict with others. Therefore, an appropriate modification amount should be selected as a reasonable compromise for all the factors at given radial clearances.

Fig. 15 shows the comparisons of optimization results of the contact stress along tooth profile between positive and negative combined modifications. The meshing tooth profile decreases with the increasing radial clearance, as expected. Also, the tooth profile in contact is less for negative combined modification, as compared with positive combined modification, which results in larger MSC.

Table 2 Optimization results for positive and negative combined TPM

Max. contact stress						
c_r / μm	Min. value / MPa	$\Delta\rho$ / μm	Δa / μm	Min. value / MPa	$\Delta\rho$ / μm	Δa / μm
10	693.460	29	19	948.578	0	–10
20	742.545	49	29	951.865	–20	–40
30	959.360	50	20	948.203	–20	–50
40	976.309	40	0	1133.089	0	–40
Mean transmission error						
c_r / μm	Min. value / arcsec	$\Delta\rho$ / μm	Δa / μm	Min. value / arcsec	$\Delta\rho$ / μm	Δa / μm
10	45.026	10	0	7.776	–13	–23
20	87.286	20	0	8.912	–27	–47
30	128.318	30	0	44.688	–20	–50
40	169.283	40	0	87.628	–10	–50
Peak-peak gear ratio						
c_r / μm	Min. value / torque ripple	$\Delta\rho$ / μm	Δa / μm	Min. value / torque ripple	$\Delta\rho$ / μm	Δa / μm
10	0.048 (0.123%)	22	12	1.335(3.423%)	–8	–18
20	0.049 (0.125%)	49	29	0.248(0.636%)	–22	–42
30	1.320 (3.384%)	41	11	0.236(0.605%)	–18	–48
40	1.249 (3.203%)	40	0	3.790(9.718%)	–10	–50

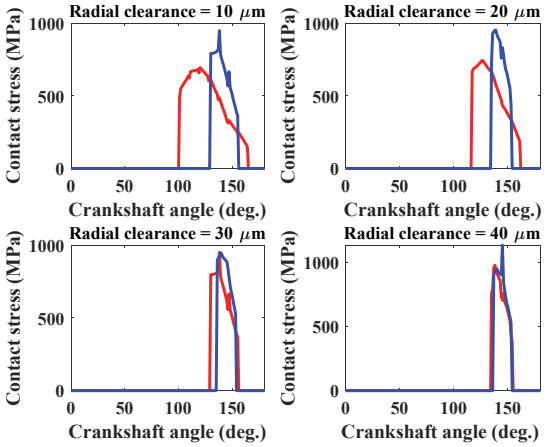

Figure 15 Comparisons of optimization results of contact stress along tooth profile positive (——) and negative (——) combined modifications

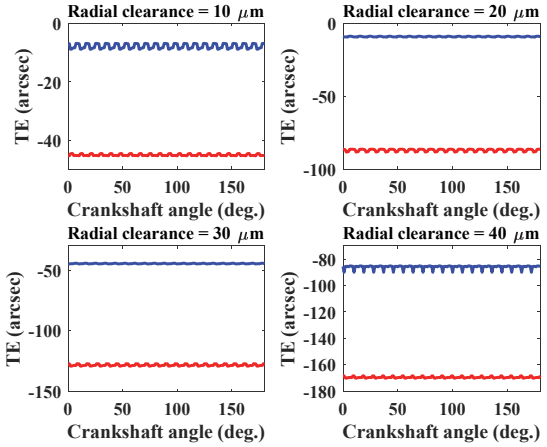

Figure 16 Comparisons of optimization results of *TE* between positive (——) and negative (——) combined modifications

Fig. 16 shows the comparisons of optimization results of the loaded *TE* between positive and negative combined modifications. It is observed that the mean values of the loaded *TE* will increase with the increasing radial clearances. Note that for the negative combined modification, the mean value of the loaded *TE* shows much smaller than those of the positive combined modification while the PPTE is larger at some radial clearances. It suggests that the cycloid drive tends to obtain higher location accuracy with negative combined modification.

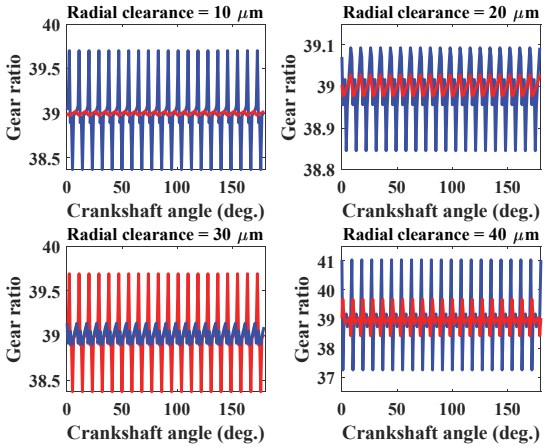

Figure 17 Comparisons of optimization results of GR between positive (——) and negative (——) combined modifications

Fig. 17 shows the comparisons of optimization results of *GR* between positive and negative combined modifications, where large discrepancies are observed. It is found that for some cases of optimal TPM, the values of PPGR are ranging from 3.2% to 9.7 % of the ideal *GR*. The fluctuation of *GR* is the main reason for the torque ripple, which will lead to the harmonic resonance of the industrial robot. To avoid this, appropriate modification types and amounts should be chosen in the design process.

6 CONCLUSION

In this study, to simulate and predict the multi-tooth contact characteristics of cycloid drives with TPM, a load distribution model is proposed, which is verified by comparing with the FEM results. Four types of TPMs are proposed and the constrain conditions are also discussed. A numerical example of the cycloid gear without TPM and with TPM is studied. The comparison shows significant influences of tooth profile modifications on the performances of the cycloid drive. A methodology based on the proposed model is developed to identify the optimal TPM at given radial clearances. The two-dimensional

parameter map is used for the minimization of MCS, MTE and PPGR. The comparisons of optimization results of two combined modifications at the same radial clearances yield the following conclusions: 1. For the modifications considered, the loaded *TE* increases as the radial clearance increases. 2. Negative combined modification tends to produce smaller *TE* than positive combined modification. 3. For both two combined modifications, the values of PPGR are apt to have a wide range of variation, which should be considered significantly in the design process. This study provides some guidelines for the design, analysis, and optimization of cycloid drives.

Acknowledgements

This research was funded by the National Natural Science Foundation of China (Grant No. 52005354), the Natural Science Foundation of Jiangsu Province (Grant No. BK20190824).

7 REFERENCES

[1] Wang, H., Shi, Z. Y., Yu, B., & Xu, H. (2019). Transmission performance analysis of RV reducers influenced by profile modification and load. *Applied Sciences*, *9*(19), 4099. https://doi.org/10.3390/app9194099

[2] Kumar, N., Kosse, V., & Oloyede, A. (2016). A new method to estimate effective elastic torsional compliance of single-stage cycloidal drives. *Mechanism and Machine Theory*, *105*, 185-198. https://doi.org/10.1016/j.mechmachtheory.2016.06.023

[3] Gorla, C., Davoli, P., Rosa, F., Longoni, C., Chiozzi, F., & Samarani, A. (2008). Theoretical and experimental analysis of a cycloidal speed reducer. *Journal of Mechanical Design*, *130*(11), 112604. https://doi.org/10.1115/1.2978342

[4] Yang, D. C. H. & Blanche, J. G. (1990). Design and application guidelines for cycloid drives with machining tolerances. *Mechanism and Machine Theory*, *25*(5), 487-501. https://doi.org/10.1016/0094-114X(90)90064-Q

[5] Sensinger, J. W. (2010). Unified approach to cycloid drive profile, stress, and efficiency optimization. *Journal of Mechanical Design*, *132*(2), 024503. https://doi.org/10.1115/1.4000832

[6] Lin, W. S., Shih, Y. P., & Lee, J. J. (2014). Design of a two-stage cycloidal gear reducer with tooth modifications. *Mechanism and Machine Theory*, *79*, 184-197. https://doi.org/10.1016/j.mechmachtheory.2014.04.009

[7] Malhotra, S. K. & Parameswaran, M. A. (1983). Analysis of a cycloid speed reducer. *Mechanism and Machine Theory*, *18*(6), 491-499. https://doi.org/10.1016/0094-114X(83)90066-6

[8] Blagojevic, M., Marjanovic, N., Djordjevic, Z., Stojanovic, B., & Disic, A. (2011). A new design of a two-stage cycloidal speed reducer. *Journal of Mechanical Design*, *133*(8), 085001. https://doi.org/10.1115/1.4004540

[9] Li, X., Li, C, Wang, Y., Chen, B., & Lim, T. C. (2017). Analysis of a cycloid speed reducer considering tooth profile modification and clearance-fit output mechanism. *Journal of Mechanical Design*, *139*(3), 033303. https://doi.org/10.1115/1.4035541

[10] Li, X., Chen, B., Wang, Y. W., & Lim, T. C. (2018). Mesh stiffness calculation of cycloid-pin gear pair with tooth profile modification and eccentricity error. J*ournal of Central South University*, *25*(7), 1717-1731. https://doi.org/10.1007/s11771-018-3863-z

[11] Xu, L. X., Chen, B. K., & Li, C. Y. (2019). Dynamic modelling and contact analysis of bearing-cycloid-pinwheel transmission mechanisms used in joint rotate vector reducers. *Mechanism and Machine Theory*, *137*, 432-458. https://doi.org/10.1016/j.mechmachtheory.2019.03.035

[12] Sun, X., Han, L., & Wang, J. (2019). Design and transmission error analysis of CBR reducer. *Journal of Mechanical Design*, *141*(8), 082301. https://doi.org/10.1115/1.4043368

[13] Lin, K. S., Chan, K. Y., & Lee, J. J. (2018). Kinematic error analysis and tolerance allocation of cycloidal gear reducers. *Mechanism and Machine Theory*, *124*, 73-99. https://doi.org/10.1016/j.mechmachtheory.2017.12.028

[14] Li, T., An, X., Deng, X., Li, J., & Li, Y. (2020). A new tooth profile modification method of cycloidal gears in precision reducers for robots. *Applied Sciences*, *10*(4), 1266. https://doi.org/10.3390/app10041266

[15] Hsieh, C. F. & Fuentes-Aznar, A. (2019). Performance prediction method of cycloidal speed reducers. *Journal of the Brazilian Society of Mechanical Sciences & Engineering*, *41*(4), 186. https://doi.org/10.1007/s40430-019-1690-2

[16] Li, S. (2014). Design and strength analysis methods of the trochoidal gear reducers. *Mechanism and Machine Theory*, *81*, 140-154. https://doi.org/10.1016/j.mechmachtheory.2014.07.001

[17] Kim, K. H., Lee, C. S., & Ahn, H. J. (2009). Torsional Rigidity of a Cycloid Drive Considering Finite Bearing and Hertz Contact Stiffness. *ASME 2009 International Design Engineering Technical Conferences and Computers and Information in Engineering Conference.* https://doi.org/10.1115/DETC2009-87092

[18] Chen, B. K., Zhong, H., Liu, J., Li, C., & Fang, T. (2012). Generation and investigation of a new cycloid drive with double contact. *Mechanism and Machine Theory*, *49*, 270-283. https://doi.org/10.1016/j.mechmachtheory.2011.10.001

[19] Litvin, F. L. & Feng, P. H. (1996). Computerized design and generation of cycloidal gearings. *Mechanism and Machine Theory*, *31*(7), 891-911. https://doi.org/10.1016/0094-114X(95)00115-F

[20] Hwang, Y.W. & Hsieh, C. F. (2007). Geometric design using hypotrochoid and no undercutting conditions for an internal cycloidal gear. *Journal of Mechanical Design*, *129*(4), 413-420. https://doi.org/10.1115/1.2437806

[21] Litvin, F. L. & Fuentes, A. (2004). *Gear Geometry and Applied Theory*. Cambridge University Press: New York, USA.

Contact information:

Haidong HE, PhD, Associate Professor
School of Mechanical and Electrical Engineering, Soochow University,
Suzhou 215021, China
E-mail: hdhe@suda.edu.cn

Xuan LI, PhD, Associate Professor
(Corresponding author)
School of Mechanical and Electrical Engineering, Soochow University,
Suzhou 215021, China
E-mail: xuanli@suda.edu.cn

Ting ZHANG, PhD, Professor
School of Mechanical and Electrical Engineering, Soochow University,
Suzhou 215021, China
E-mail: tzhang@suda.edu.cn